Low-frequency 1/f noise in MoS2 transistors: Relative contributions of the channel and contacts

J. Renteria, R. Samnakay, S. L. Rumyantsev, C. Jiang, P. Goli, M. S. Shur, and A. A. Balandin

---

Articles you may be interested in

Characterization of metal contacts for two-dimensional MoS2 nanoflakes
Appl. Phys. Lett. **103**, 232105 (2013); 10.1063/1.4840317

Plasmonic enhancement of photocurrent in MoS2 field-effect-transistor
Appl. Phys. Lett. **102**, 203109 (2013); 10.1063/1.4807658

p-channel thin-film transistors based on spray-coated Cu2O films
Appl. Phys. Lett. **102**, 163505 (2013); 10.1063/1.4803085

Low-frequency noise in amorphous indium-gallium-zinc oxide thin-film transistors from subthreshold to saturation
Appl. Phys. Lett. **97**, 122104 (2010); 10.1063/1.3491553

Low-frequency noise in a thin active layer -Si:H thin-film transistors
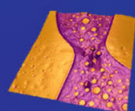J. Appl. Phys. **85**, 7952 (1999); 10.1063/1.370614
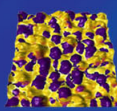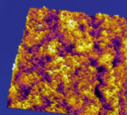
Low-frequency 1/*f* noise in MoS₂ transistors: Relative contributions of the channel and contacts

J. Renteria,[1,a)] R. Samnakay,[2,a)] S. L. Rumyantsev,[3,4] C. Jiang,[1] P. Goli,[1,2] M. S. Shur,[3] and A. A. Balandin[1,2,b)]

[1]*Nano-Device Laboratory, Department of Electrical Engineering, Bourns College of Engineering, University of California – Riverside, Riverside, California 92521, USA*
[2]*Materials Science and Engineering Program, Bourns College of Engineering, University of California – Riverside, Riverside, California 92521, USA*
[3]*Department of Electrical, Computer, and Systems Engineering, Center for Integrated Electronics, Rensselaer Polytechnic Institute, Troy, New York 12180, USA*
[4]*Ioffe Physical-Technical Institute, St. Petersburg 194021, Russia*

We report on the results of the low-frequency (1/*f*, where *f* is frequency) noise measurements in MoS₂ field-effect transistors revealing the relative contributions of the MoS₂ channel and Ti/Au contacts to the overall noise level. The investigation of the 1/*f* noise was performed for both as fabricated and aged transistors. It was established that the McWhorter model of the carrier number fluctuations describes well the 1/*f* noise in MoS₂ transistors, in contrast to what is observed in graphene devices. The trap densities extracted from the 1/*f* noise data for MoS₂ transistors, are $2 \times 10^{19}\,eV^{-1}cm^{-3}$ and $2.5 \times 10^{20}\,eV^{-1}cm^{-3}$ for the as fabricated and aged devices, respectively. It was found that the increase in the noise level of the aged MoS₂ transistors is due to the channel rather than the contact degradation. The obtained results are important for the proposed electronic applications of MoS₂ and other van der Waals materials. © *2014 AIP Publishing LLC*. [http://dx.doi.org/10.1063/1.4871374]

Recent advances in the exfoliation and growth of two-dimensional (2D) layered materials have allowed for investigation of their electronic and optical properties.[1–4] Among these material systems, molybdenum disulfide (MoS₂) is one of the more stable layered transition-metal dichalcogenides (TMDCs).[5,6] Each layer of MoS₂ consists of one sub-layer of molybdenum sandwiched between two other sub-layers of sulfur in a trigonal prismatic arrangement.[7] A single-layer MoS₂ shows a direct band gap of ∼1.9 eV, while bi-layer and bulk MoS₂ exhibit an indirect band gap of ∼1.6 eV and ∼1.3 eV, respectively.[8–10] It has been demonstrated that bi- and few-layer MoS₂ devices are promising for sensing, opto-electronic, and energy harvesting applications.[11–13] Owing to its relatively large energy band gap, the MoS₂ field-effect transistors (FETs) offer reasonable on-off ratios, which suggests possibilities for digital or analog electronic applications of this 2D *van der Waals* material.[13,14]

Like other material systems, practical applications of MoS₂ devices in sensing and in digital or analog electronics are only possible if the material and devices meet the minimum level requirements for low-frequency 1/*f* noise.[15–23] The sensitivity of amplifiers and transducers used in sensors is ultimately defined by the flicker (1/*f*) noise.[23] The accuracy of a system limited by 1/*f* noise cannot be improved by extending the measuring time, *t*, because the total accumulated energy of the 1/*f* noise increases at least as fast as the measuring time *t*. In contrast, the system accuracy limited by white noise, e.g., shot or thermal noise, increases the measuring time as $t^{1/2}$. For

this reason, the sensitivity and selectivity of many types of sensors, particularly those that rely on electrical response, is limited by 1/*f* noise. Although 1/*f* noise dominates the noise spectrum only at low frequencies, its level is equally important for electronic applications at high frequencies, because 1/*f* noise is the major contributor to the phase noise of the oscillating systems. The up-conversion of 1/*f* noise is a result of unavoidable non-linearity in devices and the electronic systems, which leads to phase noise contributions.

Meeting the requirements for 1/*f* noise level could be particularly challenging for 2D materials, where the electrons in the conducting channels are ultimately exposed to the charged traps in the gate dielectrics and substrates.[24] The contributions of contacts to the low-frequency noise can also be significant owing to imperfection of the technology for metal deposition on TMDCs. Investigations of the low-frequency 1/*f* noise in MoS₂ devices are in its infancy,[25–27] and many questions regarding the specific physical mechanism of 1/*f* noise in this material remained unanswered, including the role of metal contacts and aging. The nanometer-scale thickness of the device channel may change the noise level compared to devices with conventional feature sizes.[19–24] In this letter, we address these issues while focusing on separating the contributions from the MoS₂ channel and Ti/Au contacts to the overall noise level. The devices selected for this study used bi-layer and tri-layer MoS₂ films, because they are more robust for practical electronic applications.

Thin films of MoS₂ were exfoliated from bulk crystals and transferred onto Si/SiO₂ substrates following the standard "graphene-like" approach.[28–30] The thickness *H* of the films ranged from bi-layer to a few layers. Micro-Raman

---

a)J. Renteria and R. Samnakay contributed equally to this work.
b)Author to whom correspondence should be addressed. Electronic mail: balandin@ee.ucr.edu.

spectroscopy (Renishaw InVia) verified the crystallinity and thickness of the flakes after exfoliation. It was performed in the backscattering configuration under $\lambda = 488$-nm laser excitation laser using an optical microscope (Leica) with a $50\times$ objective. The excitation laser power was limited to less than 0.5 mW to avoid local heating. In Figure 1, we present informative bands at $\sim 382.9\,\text{cm}^{-1}$ (E^1_{2g}) and $406.0\,\text{cm}^{-1}$ (A_{1g}), consistent with the previous reports of the MoS_2 Raman spectrum.[31] Analysis of the Raman spectrum indicates that this sample is a tri-layer MoS_2 film. The latter follows from the frequency difference, $\Delta\omega$, between the E^1_{2g} and the A_{1g} peaks. The increase in the number of layers in MoS_2 films is accompanied by the red shift of the E^1_{2g} and blue shift of the A_{1g} peaks.[31] This sensitivity of the Raman spectral features of MoS_2 to the film thickness was used to reliably determine the thickness of the samples used for fabricating FETs.

Devices with MoS_2 channels were fabricated using electron beam lithography (LEO SUPRA 55) for patterning of the source and drain electrodes and the electron-beam evaporation (Temescal BJD-1800) for metal deposition. Conventional Si substrates with 300-nm thick SiO_2 layers were spin coated (Headway SCE) and baked consecutively with two positive resists: first, methyl methacrylate (MMA) and then, polymethyl methacrylate (PMMA). These devices consisted of MoS_2 thin-film channels with Ti/Au (10-nm/100-nm) contacts. The heavily doped Si/SiO_2 wafer served as a back gate. Inset in Figure 1 shows a scanning electron microscopy (SEM) image of representative MoS_2 – Ti/Au devices. The majority of the bi-layer and tri-layer thickness devices had a channel length, L, in the range from $1.3\,\mu\text{m}$ to $3.5\,\mu\text{m}$, and the channel width, W, in the range from $1\,\mu\text{m}$ to $7\,\mu\text{m}$.

Figures 2(a)–2(c) show the room-temperature (RT) current-voltage (I-V) characteristics of the fabricated MoS_2 devices. Figure 2(a) presents repeated sweeps of the source-drain voltage in the range from $-0.1\,\text{V}$ to $+0.1\,\text{V}$. The linear I-V characteristics suggest that the MoS_2 – Ti/Au
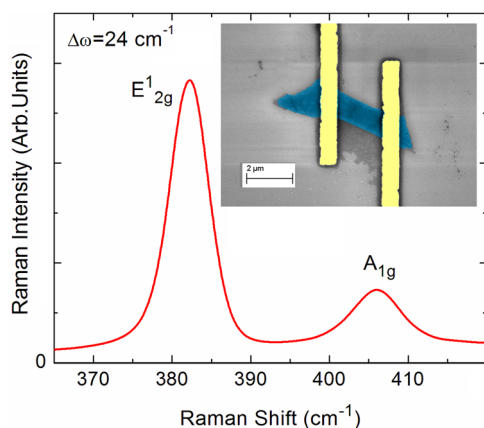

FIG. 1. Raman spectrum of an MoS_2 thin film showing the E^1_{2g} and the A_{1g} peaks. The increase in the number of layers in MoS_2 films is accompanied by the red shift of the E^1_{2g} and blue shift of the A_{1g} peaks. The energy difference, $\Delta\omega$, between E^1_{2g} and the A_{1g} peaks indicates that the given sample is a tri-layer MoS_2 film. Inset shows a SEM image of a representative MoS_2 – Ti/Au field-effect transistor. The pseudo colors are used for clarity: yellow corresponds to the metal contacts while blue corresponds to MoS_2 thin-film channel.
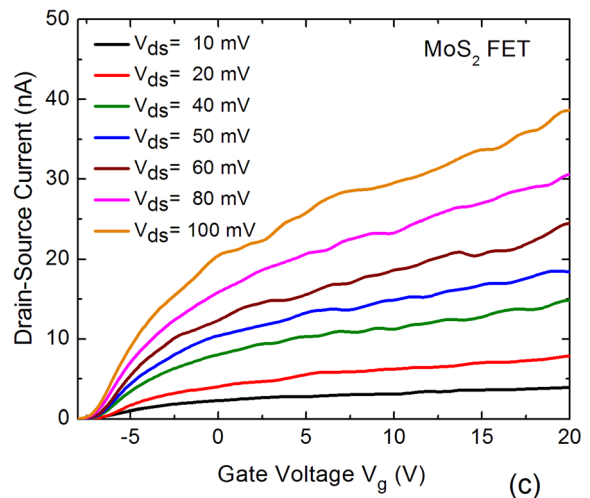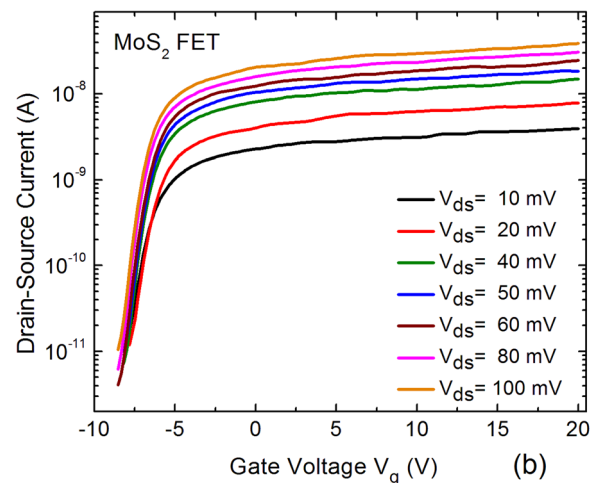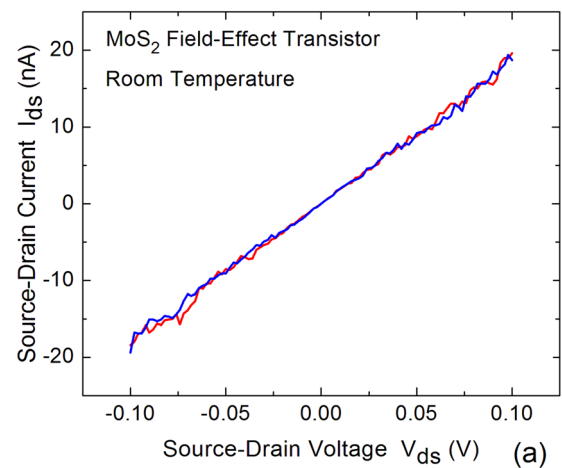

FIG. 2. Current-voltage characteristics of the fabricated MoS_2 FET at room temperature. The drain-source current for repeated sweeps of the source-drain voltage in the small-voltage range between $-0.1\,\text{V}$ and $+0.1\,\text{V}$ at $V_g = 0\,\text{V}$ (a). The drain-source current, I_{ds}, shown as a function of the back-gate bias, V_g, in the semi-log (b), and linear scale (c).

contacts are Ohmic. Figures 2(b) and 2(c) show the drain-source current, I_{ds}, as a function of the back-gate bias, V_g, in the semi-log and linear scale, respectively. As seen, the device behaves as an n-channel field effect transistor. The curves of different colors correspond to the source-drain bias, V_{ds}, varying from $10\,\text{mV}$ to $100\,\text{mV}$. As seen from

Figure 2(b), a representative device reproducibly reveals a well-defined threshold voltage, $V_{th} = (-7)$–(-8) V obtained from the linear extrapolation of I_d versus V_g characteristics (in the linear scale). The threshold voltage varied from device to device depending on channel size. It steadily shifted more negative as a result of aging. The current on/off ratio greater than 6.6×10^3 was determined at a drain-source bias of 80 mV. We deduced a subthreshold slope of 549 mVdec^{-1} at the bias of $V_{ds} = 100$ mV.

In Figure 3, we compare the transfer I-V characteristics and calculated effective mobility for as fabricated and aged transistors. Aging results in the threshold voltage shift from $V_{th} = -7$ V to $V_{th} = -7.5$ V and a current increase at high gate voltages. A rough estimate for the total contact resistances, R_C, can be obtained by plotting the drain-to-source resistance, R_{ds}, versus $1/(V_g\text{-}V_{th})$, and extrapolating this dependence to zero as shown in the inset to Figure 3. For this particular device, the procedure yields the contact resistance of $R_C \approx 2$ MΩ and $R_C \approx 1.5$ MΩ for as fabricated and aged devices, respectively. The contact resistance, R_C extracted from the intercepts in the inset to Figure 3 was used for the effective mobility calculation:[35]

$$\mu_{eff} = \frac{L_g}{C_{OX}(R_{ds} - R_C)(V_g - V_{th})W}. \tag{1}$$

Here, $C_{OX} = \varepsilon_o\varepsilon_r/d = 1.15 \times 10^{-4}$ (F/m^2) is the oxide capacitance, where ε_o is the dielectric permittivity of free space, ε_r is the dielectric constant and d is the oxide thickness. We used $\varepsilon_r = 3.9$ and $d = 300$ nm for the SiO$_2$ layer. As seen from Figure 3, the extracted effective mobility is virtually the same for virgin and aged devices, and only weakly depends on the gate voltage. The uncertainty in the value of the contact resistance results in the uncertainty of the calculated mobility. However, the values of the mobility obtained for this and all other devices were in the range of 1–8 cm^2/Vs, which is typical for similarly fabricated MoS$_2$ FETs.[11,14,32–34] For the noise trap density analysis the exact value of the contact resistance is not so important, as will be shown later.
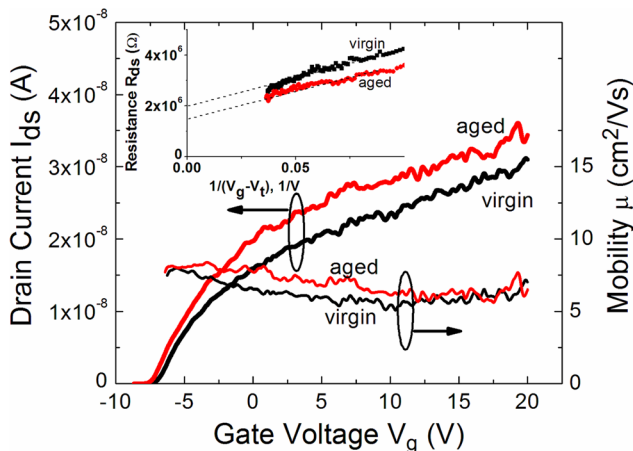
The noise was measured in the linear region at $V_d = 50$ mV keeping the source at the ground potential. The voltage fluctuations from the drain load resistance of $R_L = 50$ kΩ were analyzed with a dynamic signal analyzer (SR785). The measurements were conducted under ambient conditions at room temperature. Figure 4 shows typical low-frequency noise spectra of voltage fluctuations, S_v, as a function of frequency for several values of drain-source and gate biases. One can see that the low-frequency noise is of the $1/f$ type without any signatures of generation-recombination bulges. To verify how closely the noise spectral density follows $1/f$ dependence, we fitted the experimental data with $1/f^\alpha$. The parameter α varied in the range from $\sim$0.75 to $\sim$1.25 without revealing any clear gate bias, V_g, dependence. The latter suggests that the traps contributing to the noise distributed uniformly in space and energy.[23]

For any material technology, it is important to analyze the relative contributions of the device channel and contacts as well as to assess the effects of aging. To accomplish this goal, we calculated the short-circuit current fluctuations in the usual way as $S_I = S_v[(R_L + R_{ds})/(R_L R_{ds})]^2$, where R_L and R_D are the load and device resistances, respectively. The noise spectrum density at different drain-source biases was consistently proportional to the current squared at a constant gate voltage V_g: $S_I \sim I_{ds}^2$. The latter implies that the current does not drive the fluctuations but merely makes the fluctuations in the sample visible via Ohm's law.[19] The noise was measured in the same devices within the span of two weeks. As a result of aging, the threshold voltage shifted to a more negative value and total drain to source resistance decreased. The circular symbols in Figure 5 represent the normalized current noise, S_I/I_{ds}^2, as a function of the gate bias for the as fabricated device and device aged for a week in ambient atmosphere (Transfer current voltage characteristics of these devices are shown in Fig. 3). One can see that the normalized noise spectral density is an order of magnitude larger in the week old device. The latter suggests that capping of MoS$_2$ with some protective layer may be a technologically viable way for reducing $1/f$ noise for practical applications.

FIG. 3. Transfer current-voltage characteristics and effective mobility for as fabricated and one week aged transistors at $V_d = 80$ mV. The inset shows the plot of the total drain to source resistance versus $1/(V_g\text{-}V_{th})$ used for contact resistance estimate.
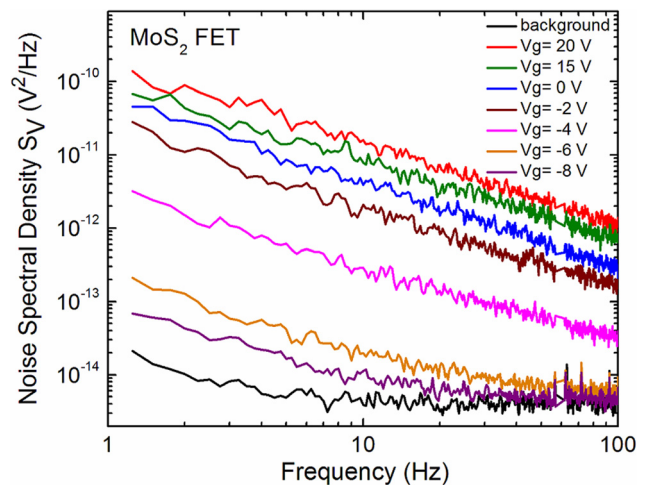

FIG. 4. Typical low-frequency noise spectra of voltage fluctuations, S_v, as a function of frequency f for different values of the gate bias. The data are for the linear regime at $V_d = 50$ mV and the source contact at a ground potential. The measurements were conducted under ambient conditions at room temperature.
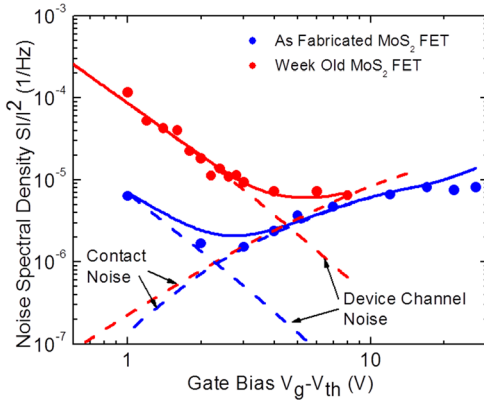
FIG. 5. Measured and simulated low-frequency noise response of MoS₂ FETs. The circular symbols represent the experimental data points for the normalized current noise spectral density, S_I/I_{ds}^2, as a function of the gate bias for the as fabricated device (blue symbols) and device aged for a week under ambient conditions (red symbols). The normalized noise spectral density is an order of magnitude larger in the week old device. The dashed lines represent the model fitting for the noise dominated by the channel contribution and, separately, by the contact contribution. The solid lines show the sum of both contributions. The agreement between the theoretical fitting and experimental data indicates that the 1/f noise in MoS₂ FETs follow the carrier number fluctuation model.

Let us now investigate the relative contribution of the metal contacts and device channels to the overall level of 1/f noise. This issue is of particular importance for MoS₂ devices due to the fact that the technology of metal contact fabrication to TMDCs is still rudimentary. Since the contact resistance is not negligible, we consider that both the metal contact and MoS₂ channel contribute to the measured noise. In this case, we can write that[23]

$$\frac{S_I}{I_{ds}^2} = \frac{S_{RCH}}{R_{CH}^2}\frac{R_{CH}^2}{(R_{CH}+R_C)^2} + \frac{S_{RC}}{R_C^2}\frac{R_C^2}{(R_{CH}+R_C)^2}. \quad (2)$$

Here, S_{RCH}/R_{CH}^2 is the noise spectral density of the channel resistance fluctuations, R_{CH} is the resistance of the channel, R_C is the contact resistance, and S_{Rc}/R_C^2 is the noise spectral density of the contacts resistance fluctuations.

Assuming that the channel noise complies with the McWhorter carrier number fluctuation model, we can write for the noise spectral density, S_{RCH}/R_{CH}^2, the following equation:[15,20]

$$\frac{S_{RCH}}{R_{CH}^2} = \frac{kTN_t}{\gamma f W L n_s^2}, \quad (3)$$

where k as the Boltzmann constant, T is the temperature, γ is the tunneling parameter taken to be $\gamma = 10^8\,\text{cm}^{-1}$, n_s is the channel concentration, and N_t is the trap density. In the strong inversion regime, the concentration n_s can be estimated as $n_s = C_{ox}(V_g\text{-}V_{th})/q$. Since the total resistance, $R_{CH} + R_C$, was measured directly, and contact resistance can be extracted from the current voltage characteristics, there are just two fitting parameters in our analysis, N_t, S_{RC}/R_C^2.

In Figure 5, we show with the dashed lines the model fitting for the noise dominated by the channel contribution and, separately, by the contact contribution (i.e., the first term and the last term in Eq. (1), respectively). The solid lines show

the sum of both contributions. The fitted values of the contact noise were determined to be $S_{RC}/R_C^2 = 0.25 \times 10^{-4}/f$, and $0.5 \times 10^{-4}/f$ for the as fabricated and aged devices, respectively (with the contact resistances $R_C = 2\,\text{M}\Omega$ and $R_C = 1.5\,\text{M}\Omega$ for the as fabricated and aged devices, respectively). The extracted trap densities are $N_t = 2 \times 10^{19}\,\text{eV}^{-1}\text{cm}^{-3}$ and $N_t = 2.5 \times 10^{20}\,\text{eV}^{-1}\text{cm}^{-3}$ for as fabricated and aged samples, respectively. The uncertainty in the trap density estimation is close to 20% (due to the inaccuracy of the contact resistance estimate which we varied within the range 1.3–2.2 MΩ for both as fabricated and aged devices). The agreement of the model fitting (Eqs. (2) and (3)) with the experimental results indicates that the *a priori* assumption of the McWhorter model description was valid. The model description allows one to clearly distinguish the contributions to the noise from the MoS₂ channel and from the metal contacts. The absolute value of the trap density extracted is within the range found in MoS₂-based transistors by other methods.[33,36]

Let us now compare the noise mechanism in MoS₂ thin-films with that in conventional semiconductors, metals, and graphene devices. It is known that 1/f noise is either due to the mobility fluctuations or the number of carriers fluctuations. In conventional semiconductor devices, such as Si complementary metal-oxide-semiconductor (CMOS) FETs, 1/f noise is described by the McWhorter model,[15] which is based on the carrier-number fluctuations. In metals, on the other hand, 1/f noise is usually attributed to the mobility fluctuations.[19] There are materials and devices where contributions from both mechanisms are comparable or cross-correlated. By assuming the McWhorter model for the MoS₂ channel noise we were able to reproduce the overall noise gate-bias dependence in MoS₂ FETs. The latter indicates that the 1/f noise mechanism in MoS₂ FETs is similar to that in conventional Si CMOS transistors: carrier number fluctuations with the traps widely distributed in space and energy. It is important to note here such 1/f noise behavior is quite different from that of another important 2D material, graphene, where the gate voltage dependence of noise does not follow the McWhorter model.[15] It was shown that 1/f noise in graphene can be more readily described by the mobility fluctuation.[24] The latter was concluded on the basis of analysis of the gate bias dependence,[37–39] effect of electron beam irradiation damage,[40] noise scaling with the thickness,[41,42] and measurements of noise in graphene devices under magnetic field.[43]

There is another important observation from the experimental data and model fitting presented in Figure 5. The amplitude of noise and corresponding trap density in the MoS₂ channel increased more than an order of magnitude as a result of aging. Meanwhile, the contact noise only slightly increased and contact resistance even decreased in the aged device. Therefore, we can conclude that aging results mainly from the deterioration of the MoS₂ channel. Contrary to our observations, the studies of the low-frequency noise in a single-layer exfoliated MoS₂ device[25] and a few-layer CVD grown MoS₂ device[26] revealed the compliance of the noise behavior with the Hooge empirical relation. On the other hand, transistors based on the multilayer exfoliated MoS₂ structures revealed the McWhorter mechanism of noise in

the accumulation mode.[27] At this point, it is not clear if these discrepancies in the noise mechanism interpretations are due to the different number of layers in the tested devices or different fabrication technology and quality of the device structures.

In conclusion, we reported results of the low-frequency noise investigation in MoS_2 FETs with Ti/Au contacts. It was established that both the channel and contacts contribute to the overall $1/f$ noise level of the as fabricated and aged transistors. The intrinsic noise characteristics in MoS_2 devices are well described by the McWhorter model of the carrier number fluctuations, in contrast to graphene devices. It was found that the increase in the noise level in aged MoS_2 transistors is due to channel rather than contact degradation. The obtained results can be used for optimization of devices with channels implemented with MoS_2 and other van der Waals materials.

[1]A. K. Geim and I. V. Grigorieva, Nature **499**, 419 (2013).
[2]M. Chhowalla, H. S. Shin, G. Eda, L.-J. Li, K. P. Loh, and H. Zhang, Nat. Chem. **5**, 263 (2013).
[3]D. Teweldebrhan, V. Goyal, and A. A. Balandin, Nano Lett. **10**, 1209 (2010).
[4]Z. Yan, C. Jiang, T. R. Pope, C. F. Tsang, J. L. Stickney, P. Goli, J. Renteria, T. T. Salguero, and A. A. Balandin, J. Appl. Phys. **114**, 204301 (2013).
[5]J. Heising and M. G. Kanatzidis, J. Am. Chem. Soc. **121**, 11720 (1999).
[6]Y. Kim, J.-L. Huang, and C. M. Lieber, Appl. Phys. Lett. **59**, 3404 (1991).
[7]J. L. Verble and T. J. Wieting, Phys. Rev. Lett. **25**, 362 (1970).
[8]S. W. Han, H. Kwon, S. K. Kim, S. Ryu, W. S. Yun, D. H. Kim, J. H. Hwang, J.-S. Kang, J. Baik, H. J. Shin, and S. C. Hong, Phys. Rev. B **84**, 045409 (2011).
[9]J. M. Salmani, Y. Tan, and G. Klimeck, in *Proceedings of the International Semiconductor Device Research Symposium* (2011), p. 1.
[10]K. F. Mak, C. Lee, J. Hone, J. Shan, and T. F. Heinz, Phys. Rev. Lett. **105**, 136805 (2010).
[11]G. Eda, H. Yamaguchi, D. Voiry, T. Fujita, M. Chen, and M. Chhowalla, Nano Lett. **11**, 5111 (2011).
[12]H. Li, Z. Yin, Q. He, H. Li, X. Huang, G. Lu, D. W. H. Fam, A. I. Y. Tok, Q. Zhang, and H. Zhang, Small **8**, 63 (2012).
[13]S. Das, H.-Y. Chen, A. V. Penumatcha, and J. Appenzeller, Nano Lett. **13**, 100 (2013).
[14]H. Wang, L. Yu, Y.-H. Lee, Y. Shi, A. Hsu, M. Chin, L.-J. Li, M. Dubey, J. Kong, and T. Palacios, Nano Lett. **12**, 4674 (2012).
[15]A. L. McWhorter, in *Semiconductor Surface Physics*, edited by R. H. Kingston (University of Pennsylvania Press, Philadelphia, 1957), pp. 207–228.
[16]F. N. Hooge, IEEE Trans. Electron Devices **41**, 1926 (1994).
[17]F. N. Hooge, Phys. Lett. A **29**, 139 (1969).
[18]M. B. Weissman, Rev. Mod. Phys. **60**, 537 (1988).
[19]P. Dutta and P. M. Horn, Rev. Mod. Phys. **53**, 497 (1981).
[20]K. K. Hung, P. K. Ko, H. Chenming, and Y. C. Cheng, IEEE Trans. Electron Devices **37**, 654 (1990).
[21]A. Van der Ziel, Proc. IEEE **76**, 233 (1988).
[22]E. Simoen, A. Mercha, C. Claeys, and E. Young, Appl. Phys. Lett. **85**, 1057 (2004).
[23]A. A. Balandin, *Noise and Fluctuations Control in Electronic Devices* (American Scientific, Los Angeles, 2002).
[24]A. A. Balandin, Nat. Nanotechnol. **8**, 549 (2013).
[25]V. K. Sangwan, H. N. Arnold, D. Jariwala, T. J. Marks, L. J. Lauhon, and M. C. Hersam, Nano Lett. **13**, 4351 (2013).
[26]Y. Wang, X. Luo, N. Zhang, M. R. Laskar, L. Ma, Y. Wu, S. Rajan, and W. Lu, in *82nd ARFTG Microwave Measurement Conference* (IEEE, 2013), pp. 1–3.
[27]J. Na, M.-K. Joo, M. Shin, J. Huh, J.-S. Kim, M. Piao, J.-E. Jin, H.-K. Jang, H. J. Choi, J. H. Shim, and G.-T. Kim, Nanoscale **6**, 433 (2014).
[28]K. S. Novoselov, A. K. Geim, S. V. Morozov, D. Jiang, Y. Zhang, S. V. Dubonos, I. V. Grigorieva, and A. A. Firsov, Science **306**, 666 (2004).
[29]K. S. Novoselov, A. K. Geim, S. V. Morozov, D. Jiang, M. I. Katsnelson, I. V. Grigorieva, S. V. Dubonos, and A. A. Firsov, Nature **438**, 197 (2005).
[30]Y. Zhang, Y.-W. Tan, H. L. Stormer, and P. Kim, Nature **438**, 201 (2005).
[31]C. Lee, H. Yan, L. E. Brus, T. F. Heinz, J. Hone, and S. Ryu, ACS Nano. **4**(5), 2695 (2010).
[32]K. S. Novoselov, D. Jiang, F. Schedin, T. J. Booth, V. V. Khotkevich, S. V. Morozov, and A. K. Geim, Two-dimensional atomic crystals, Proc. Natl. Acad. Sci. U.S.A. **102**(30), 10451–10453 (2005).
[33]S. Ghatak, A. N. Pal, and A. Ghosh, ACS Nano **5**, 7707 (2011).
[34]M. Xu, T. Liang, M. Shi, and H. Chen, Chem. Rev. **113**, 3766 (2013).
[35]M. Shur, *Introduction to Electronic Devices* (Wiley, 1995), p. 393.
[36]A. Ayari, E. Cobas, and O. Ogundadegbe, J. Appl. Phys. **101**, 014507 (2007).
[37]S. Rumyantsev, G. Liu, M. Shur, and A. A. Balandin, J. Phys.: Condens. Matter **22**, 395302 (2010).
[38]G. Xu, C. M. Torres, Jr., Y. Zhang, F. Liu, E. B. Song, M. Wang, Y. Zhou, C. Zeng, and K. L. Wang, Nano Lett. **10**, 3312 (2010).
[39]Y. Zhang, E. E. Mendez, and X. Du, ACS Nano **5**, 8124 (2011).
[40]M. Z. Hossain, S. Rumyantsev, M. S. Shur, and A. A. Balandin, Appl. Phys. Lett. **102**, 153512 (2013).
[41]G. Liu, S. Rumyantsev, M. S. Shur, and A. A. Balandin, Appl. Phys. Lett. **100**, 033103 (2012).
[42]G. Liu, S. Rumyantsev, M. S. Shur, and A. A. Balandin, Appl. Phys. Lett. **102**, 093111 (2013).
[43]S. L. Rumyantsev, D. Coquillat, R. Ribeiro, M. Goiran, W. Knap, M. S. Shur, A. A. Balandin, and M. E. Levinshtein, Appl. Phys. Lett. **103**, 173114 (2013).